Supplementary Information

A two-state activation mechanism controls the histone methyltransferase Suv39h1

Manuel M. Müller[1], Beat Fierz[1]†, Lenka Bittova[1], Glen Liszczak[1], and Tom W. Muir[1]*

[1]Department of Chemistry, Princeton University, Princeton, NJ 08544, United States.

*Correspondence to: muir@princeton.edu.

†Current address: Ecole polytechnique fédérale de Lausanne, CH-1015 Lausanne, Switzerland.

SUPPLEMENTARY RESULTS

Supplementary Figure 1

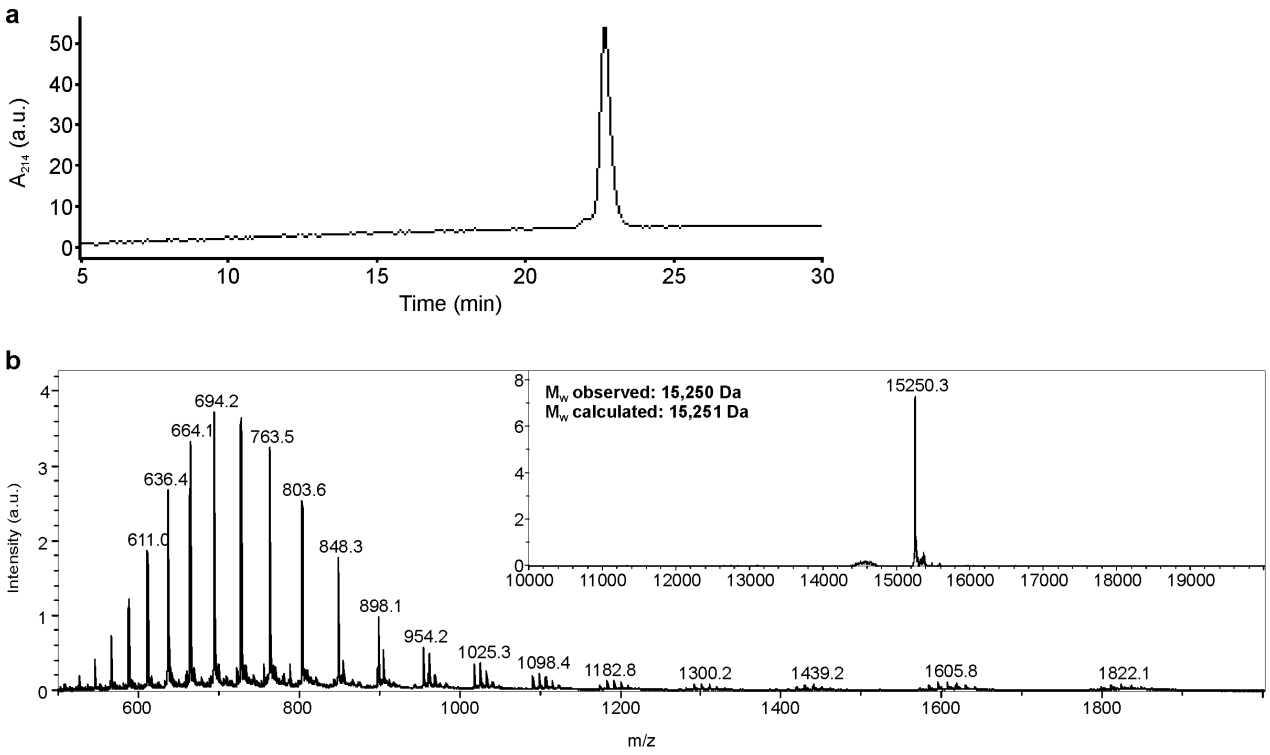

Supplementary Figure 1: Quality control of semi-synthetic histone hH3.1K9me3. (**a**) Reverse-phase HPLC of purified H3.1K9me3. (**b**) Mass spectrum of purified H3.1K9me3. The deconvoluted spectrum is depicted in the inset.

Supplementary Figure 2

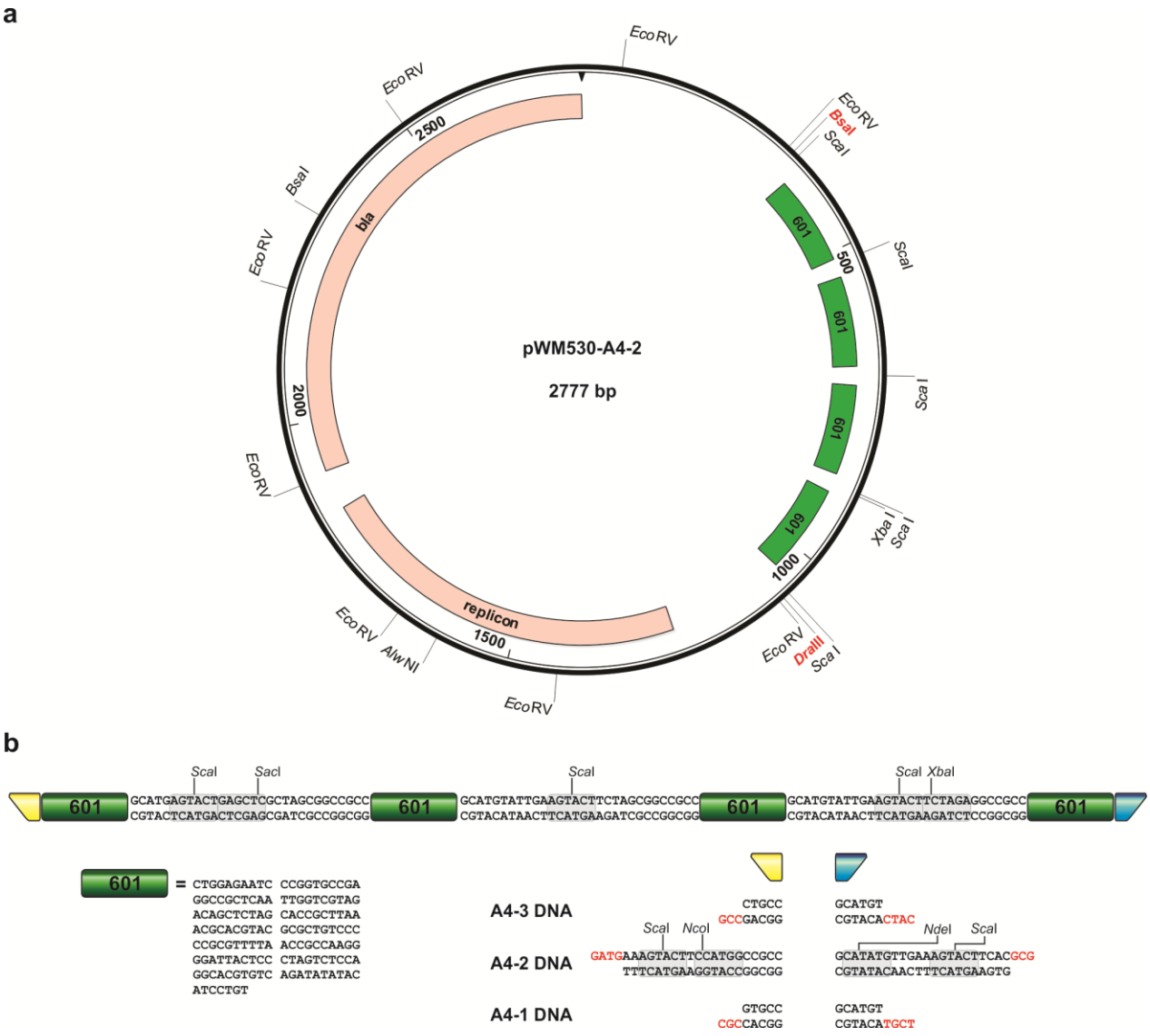

Supplementary Figure 2: Schematic of 4-mer repeat DNA sequences. (**a**) Plasmid map of pWM530 containing 4 repeats of the 601 sequence with 30 bp linkers, flanked by non-palindromic restriction sites. (**b**) DNA sequence of 4-mer repeats. Restriction sites are shaded in gray; overhangs from *AlwN*I- (**A4-1**), *Bsa*I- (**A4-1**, **A4-2**, **A4-3**) and *Dra*III- (**A4-2**, **A4-3**) digestions are depicted in red (sequence) or indicated by yellow and blue wedges (schematic). For clarity, only one strand of the 601 repeat sequence (green) is shown.

Supplementary Figure 3

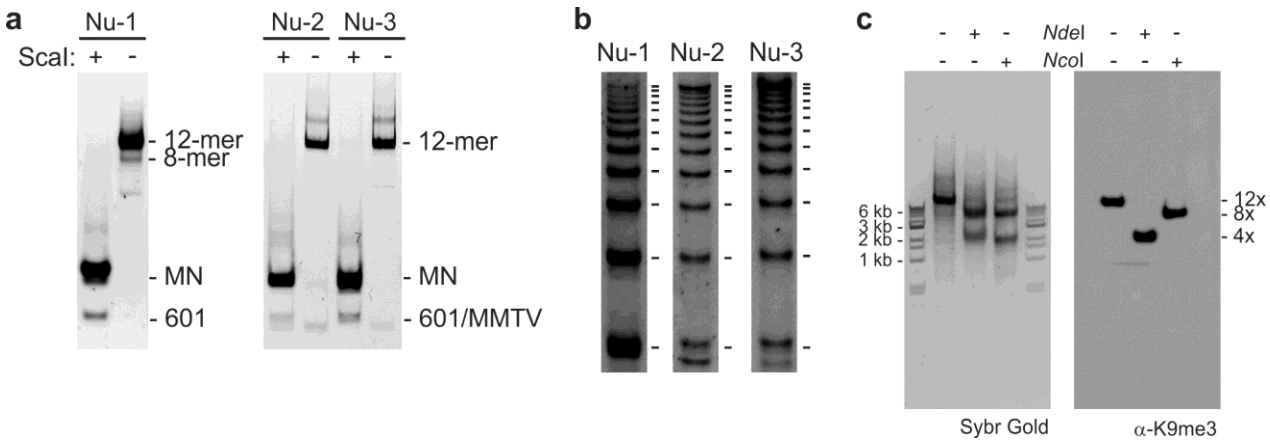

Supplementary Figure 3: Quality control of designer chromatin. (**a**) *Sca*I digestion of arrays **Nu-1**–**Nu-3**. Digests were analyzed by gel electrophoresis (1% agarose, 1% acrylamide) and Sybr Gold staining. Note that the outer nucleosomes of ligated arrays yield slightly shorter fragments than the central 177 bp repeats. MMTV corresponds to a DNA fragment of the mouse mammary tumor virus, which is included in the assembly of homogeneous 12-mer arrays as a buffer for excess octamers. (**b**) MNase digestion of arrays **Nu-1**–**Nu-3**. Dodecameric arrays are expected to leave a footprint corresponding to 12 individual bands, with the mononucleosome band (bottom) resolving into several distinct species. (c) Full images corresponding to the membrane cutouts shown in Figure **1e**. Ligated arrays (**Nu-1**) were digested and the resulting fragments analyzed by native gel electrophoresis and western blotting for H3K9me3.

Supplementary Figure 4

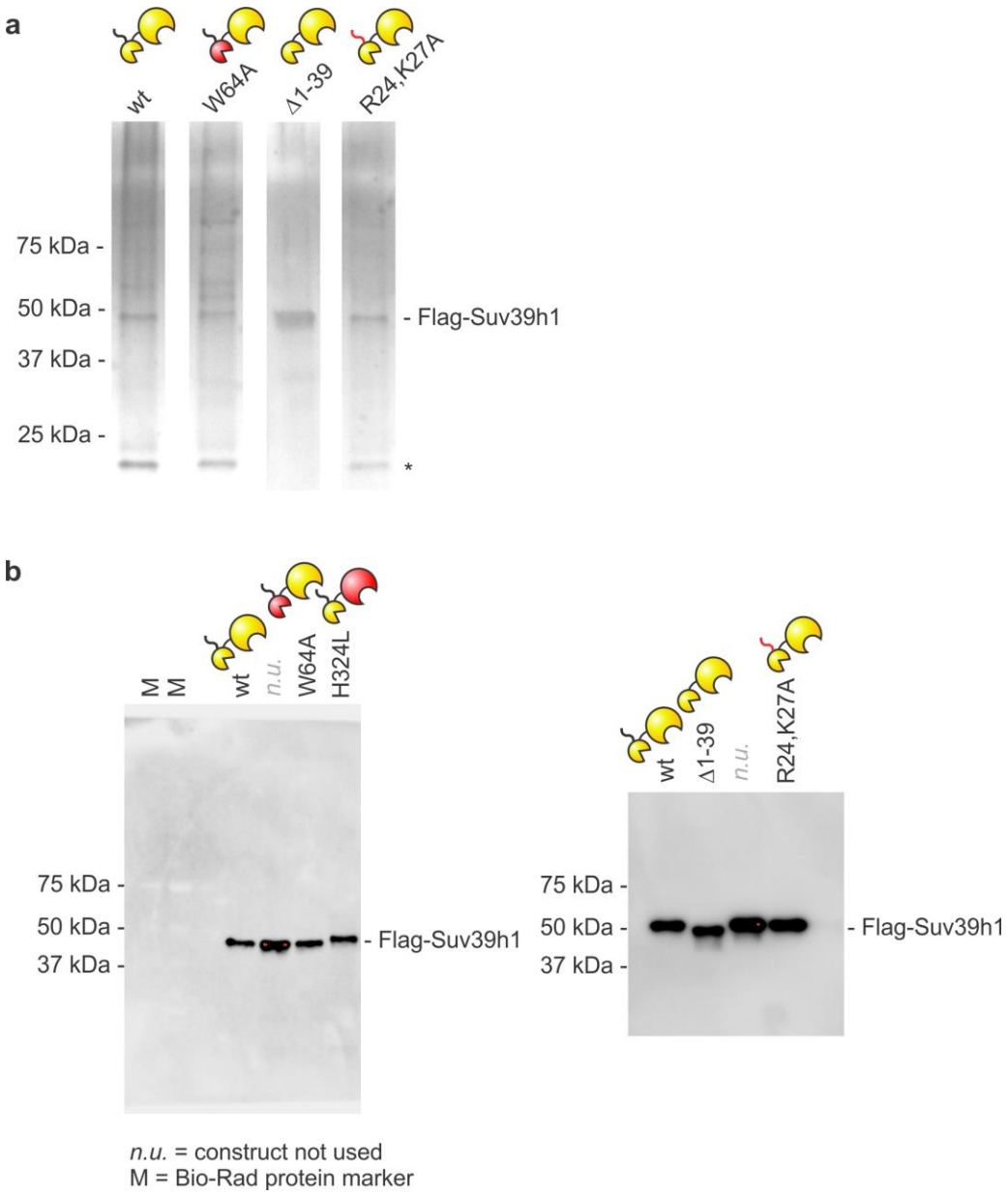

Supplementary Figure 4: Suv39h1 variants. (**a**) Silver-stained SDS-PAGE of purified Suv39h1. The band labeled with an asterisk may correspond to HP1 from *Spodoptera frugiperda* that co-purifies with Suv39h1, particularly given that it is absent in the ΔN mutant. (**b**) Anti-FLAG western blot of purified Suv39h1 variants.

Supplementary Figure 5

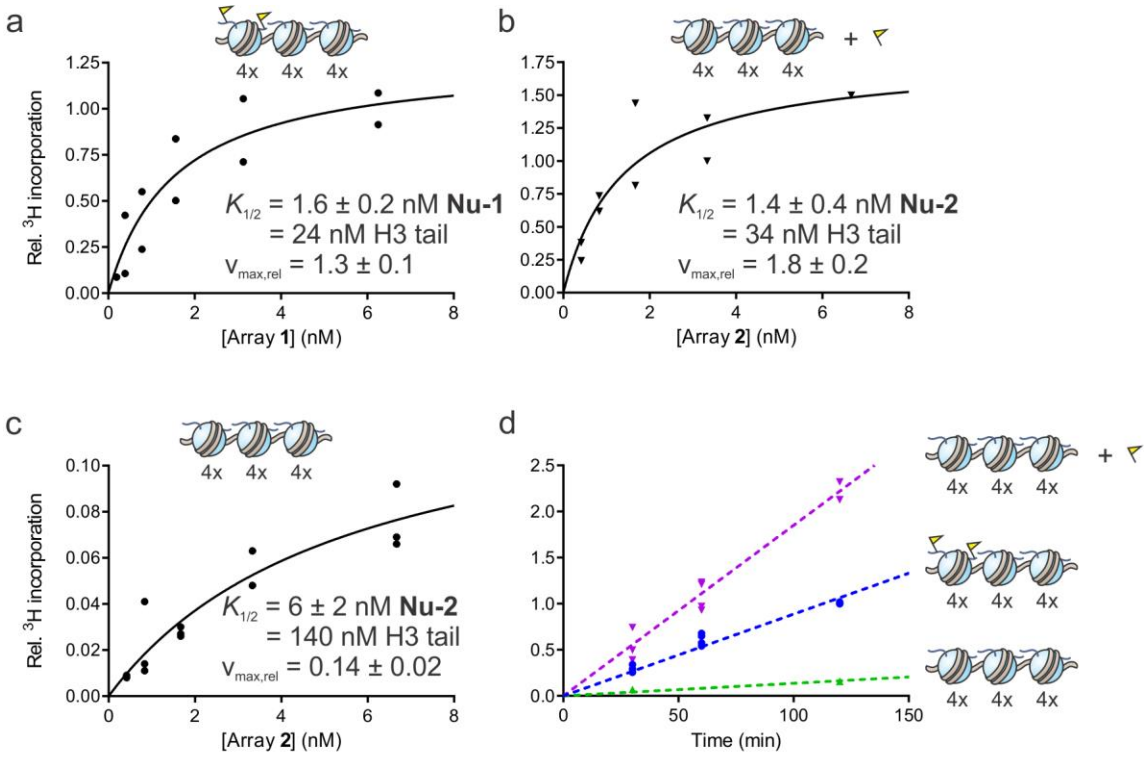

Supplementary Figure 5: Saturation kinetics of *in vitro* heterochromatin spreading. HMT activity of Suv39h1 is plotted as a function of the concentration of (a) **Nu-1**, (b) **Nu-2** in the presence of 0.2 µM H3K9me3 peptideconcentration or (c) **Nu-2** in the absence of peptide. Signals are normalized to the average scintillation count determined at 6.25 nM of **Nu-1** and **Nu-2**. Data are fitted to the Michaelis-Menten equation. The substrate concentration at which the half-maximal rate is recorded, $K_{1/2}$, and the relative maximal velocity achieved, $v_{max,rel}$ are displayed in the graphs. In panel (a), $K_{1/2}$= 1.5 ± 0.7 nM **Nu-1**, which corresponds to 18 nM 601 site or 12 nM H3K9me3-tails and 24 nM unmodified H3 tails. For comparison, Pradhan and coworkers (ref 26) reported a $K_{1/2}$ value of 0.9 ± 0.1 µM for H3 peptide substrates. (d) Time course of Suv39h1-catalyzed ^{3}H incorporation. Individual values from 2 or 3 independent replicates are shown.

Supplementary Figure 6

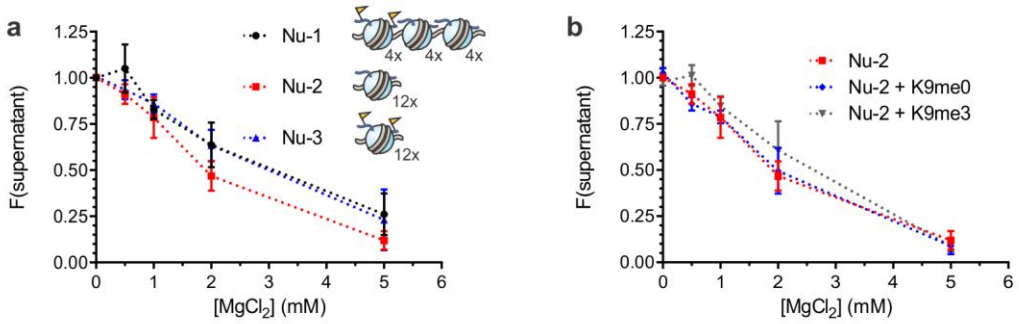

Supplementary Figure 6: Dodecameric arrays are self-assembled under HMT assay conditions. Arrays **Nu-1**–**Nu-3** (**a**) or **Nu-2** in the presence of H3 peptides (**b**) are incubated with the amount of $MgCl_2$ indicated. Upon centrifugation, the DNA content of the supernatant was analyzed by UV absorption spectroscopy or Sybr Gold fluorescence. Error bars, s.e.m. (n = 2 (**Nu-1**); n = 4 (**Nu-2** + H3K9me3); n = 3 for all other samples).

Supplementary Figure 7

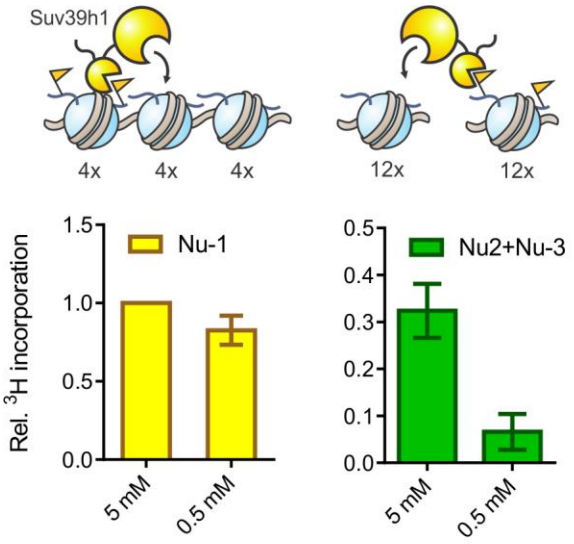

Supplementary Figure 7: Array self-assembly is important for spreading in *trans*. HMT activity of Suv39h1 with **Nu-1** (left) or a mixture or **Nu-2** and **Nu-3** (right) were performed in the presence of 0.5 or 5 mM $MgCl_2$. All values are normalized to the scintillation counts obtained with **Nu-1** at 5 mM $MgCl_2$. Error bars, s.e.m. (n = 5 (0.5 mM $MgCl_2$); n = 8 (5 mM $MgCl_2$)).

Supplementary Figure 8

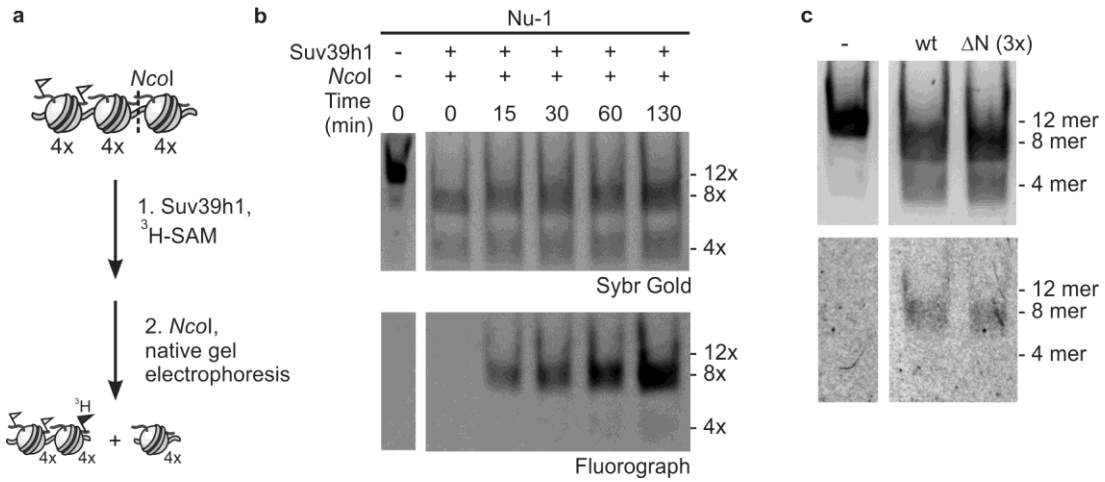

Supplementary Figure 8: Geometry of Suv39h1-catalyzed spreading steps. (**a**) Schematic of the assay. **Nu-1** was incubated in the presence of Suv39h1 and ^{3}H-SAM. After the indicated time interval, excess of cold SAM was added and the arrays digested with *Nco*I. Localization of HMT activity was determined by native gel electrophoresis and fluorography. (**b**) HMT reactions were quenched at the indicates times and the arrays were digested with *Nco*I, separated by native gel electrophoresis and analyzed by Sybr Gold staining (top) and fluorography (bottom). (**c**) Spreading geometry for wt Suv39h1 and the ΔN mutant. Note that the concentration of the ΔN was adjusted to 3x that of the wt to compensate for the slightly diminished activity.

Supplementary Figure 9

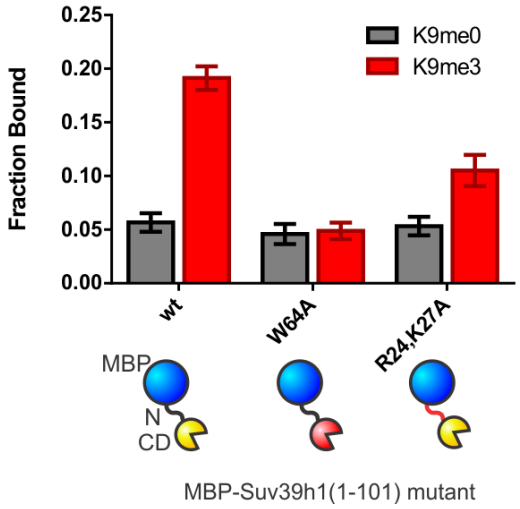

Supplementary Figure 9: H3K9me3 binding of Suv39h1 mutants. Suv39h1 fragments (residues 1–101) were fused to MBP and subjected to peptide pulldown assays. Bound proteins were analyzed by SDS-PAGE and coomassie staining, and quantified relative to a 20% input control. Error bars, s.e.m. (n = 3).

Supplementary Figure 10

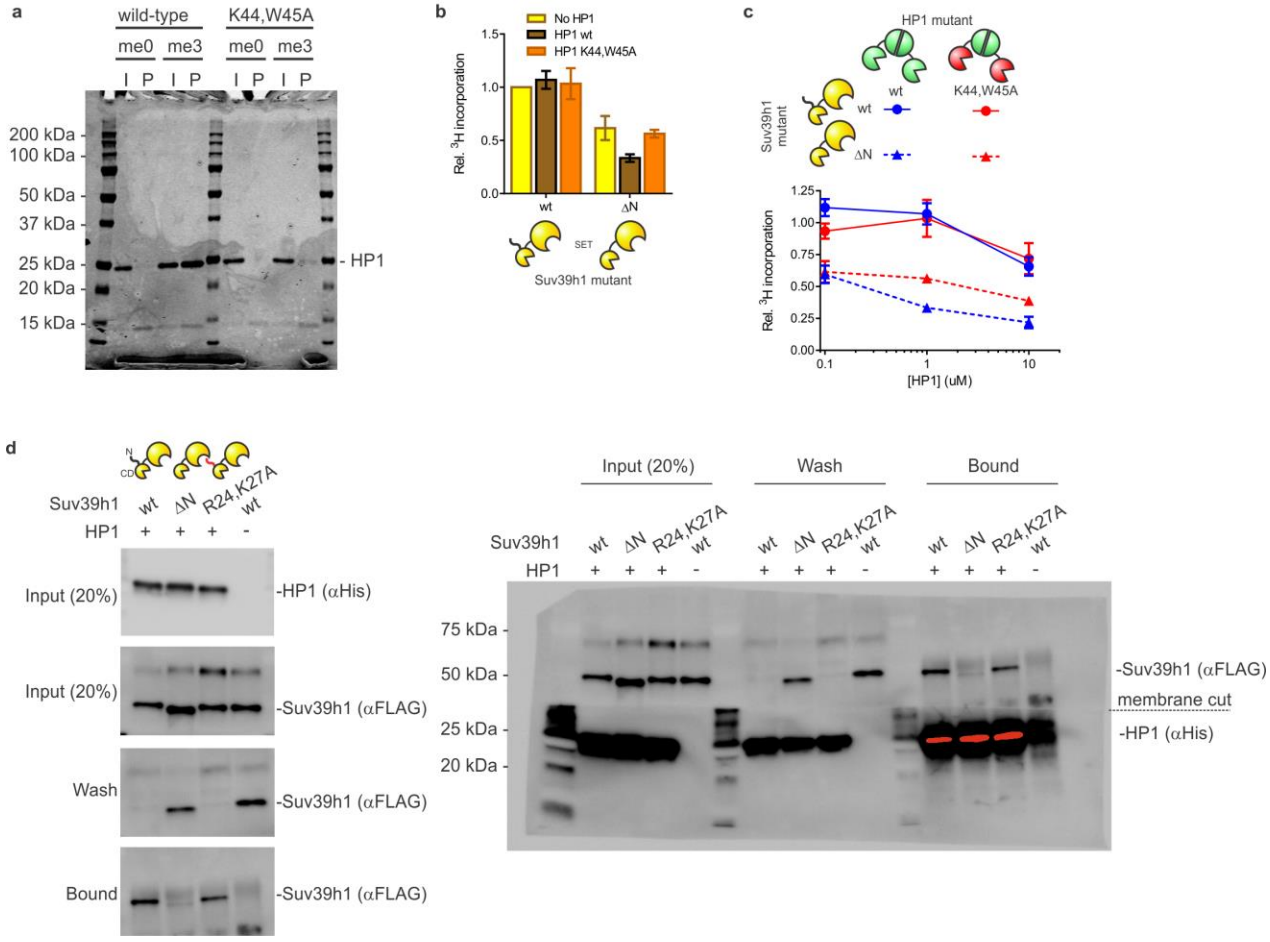

Supplementary Figure 10: Influence of HP1 on Suv39h1 activity. (a) Histone peptide binding of HP1 variants. Binding to unmodified (me0) or H3K9me3 (me3) histone peptides was evaluated by pulldown (P) of HP1 variants compared to 10 % loading controls (I). **(b)** Impact of HP1 on methylation of **Nu-1** by Suv39h1. Scintillation counts for assays in the presence of wild-type HP1 (brown) or the K44,W45A double mutant (orange) and indicated Suv39h1 variant are normalized to the values obtained for wt Suv39h1 in the absence of HP1 (yellow). Error bars, s.e.m. (n = 3-8). The reduction in Suv39h1 activity observed for the ΔN variant likely relates to competition with HP1 for the available H3K9me3 binding sites (as previously suggested, ref 13 in the main text), which can presumably be alleviated by the direct interaction of HP1 with wild-type Suv39h1. Consistent with this idea, we observed no decrease in HMT activity when a mutant HP1 containing a defective CD (K44,W45A) was added to the assay system. **(c)** Titration of HP1 (wild-type HP1: blue, K44,W45A: red) to HMT (wild-type Suv39h1: circles, ΔN: triangles) spreading assays. At 10 μM HP1, the reaction is non-specifically inhibited. Error bars, s.e.m. (n = 2–8). **(d)** HP1 binding of Suv39h1 variants. Binary interactions were evaluated using a pull-down assay via an anti-HP1 antibody. Bound and free Suv39h1 variants were measured by western blotting (α-FLAG). Cropped segments of a representative blot from 3 independent pull-down experiments are shown on the left. The original membrane is shown on the right.

Supplementary Figure 11

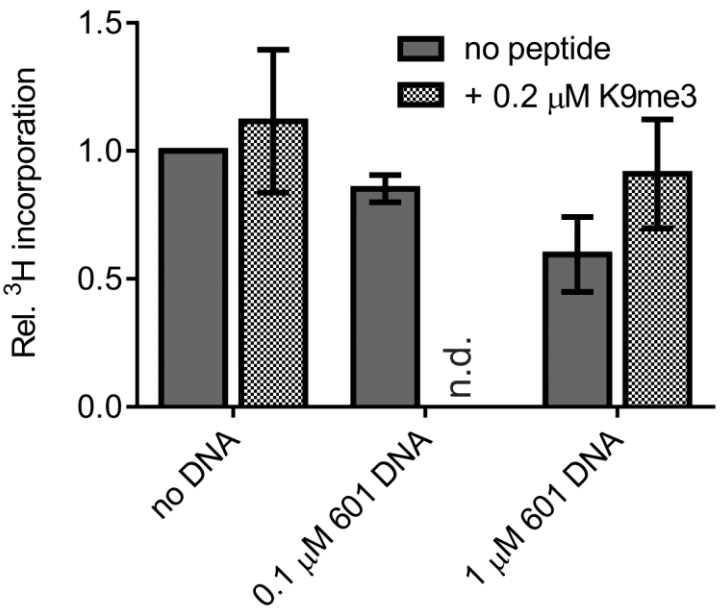

Supplementary Figure 11: DNA does not stimulate Suv39h1 activity. HMT assays with 10 μM H3K9me0 peptide were performed in the presence of 601 DNA and/or 0.2 μM H3K9me3 peptide (gray carré vs solid gray bars). Error bars, s.e.m. (n = 2 for 0.1 μM DNA samples, n = 3 for 1 μM DNA). n.d. = not determined.

Supplementary Figure 12

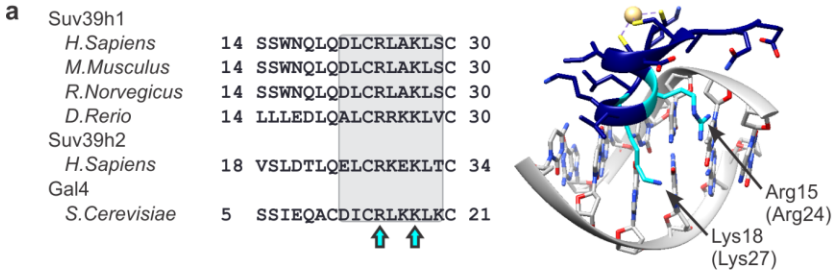

b

```
SUV91_HUMAN MAENLKGCSVCCKSSWNQLQDLCRLAKLSCPALGISKRNLYDFEVEYLCDY--KKIREQE 58
CLR4_SCHPO  ----------------------------------MSPKQEEYEVERIVDEKLDRNGAVK 25
                                                . :  ::*** : *   .:    :

SUV91_HUMAN YYLVKWRGYPDSESTWEPRQNLKCV-RILKQFHKDLERELLRRHHRSKTPRHLDPSL--- 114
CLR4_SCHPO  LYRIRWLNYSSRSDTWEPPENLSGCSAVLAEWKRR-KRRLKGSNSDSDSPHHASNPHPNS 84
             * ::*  * . ..**** :**.    :* ::::  :*.*   .  *.:*:* .

SUV91_HUMAN ------------------------------------------------------------ 114
CLR4_SCHPO  RQKHQHQTSKSVPRSQRFSRELNVKKENKKVFSSQTTKRQSRKQSTALTTNDTSIILDDS 144

SUV91_HUMAN ---------------------------------------------ANYLVQKAKQRRAL 128
CLR4_SCHPO  LHTNSKKLGKTRNEVKEESQKRELVSNSIKEATSPKTSSILTKPRNPSKLDSYTHLSFYE 204
                                                       . *

SUV91_HUMAN RR--WEQELNAKRSHLGRITVENEVDLD-GPPRAFVYINEYRVGEGITLNQV--AVGCEC 183
CLR4_SCHPO  KRELFRKKLREIEG--PEVTLVNEVDDEPCPSLDFQFISQYRLTQGVIPPDPNFQSGCNC 262
            ::  :. .*   .    .:*: **** :  *   * :*.:**: :*:   :     **:*

SUV91_HUMAN QDCLWAPTGGCCP----------GASLHKFAYNDQGQVRLRAGLPIYECNSRCRCGYDC 232
CLR4_SCHPO  SS-----LGGCDLNNPSRCECLDDLDEPTHFAYDAQGRVRADTGAVIYECNSFCSCSMEC 317
            ..      ***               .  :***: **:**  :*  ****** * *. :*

SUV91_HUMAN PNRVVQKGIRYDLCIFRTDDGRGWGVRTLEKIRKNSFVMEYVGEIITSEEAERRGQIYDR 292
CLR4_SCHPO  PNRVVQRGRTLPLEIFKTK-EKGWGVRSLRFAPAGTFITCYLGEVITSAEAAKRDKNYDD 376
            ******:*    * **:*.  :*****:*.     :*:  *:**:*** ** :* : **

SUV91_HUMAN QGATYLFDLDYVED--VYTVDAAYYGNISHFVNHSCDPNLQVYNVFIDNLDERLPRIAFF 350
CLR4_SCHPO  DGITYLFDLDMFDDASEYTVDAQNYGDVSRFFNHSCSPNIAIYSAVRNHGFRTIYDLAFF 436
            :* ******* .:*   *****  **::*:*.****.**: :*... :.  . :  :***

SUV91_HUMAN ATRTIRAGEELTFDYNMQVDPVDMESTRMDSNFGLAGLPGSPKKRVRIECKCGTESCRKY 410
CLR4_SCHPO  AIKDIQPLEELTFDYAGAKDFSPVQSQKS---------QQNRISKLRRQCKCGSANCRGW 487
            * : *:  *******    *   ::* :            .  .::* :****: .** :

SUV91_HUMAN LF- 412
CLR4_SCHPO  LFG 490
            **
```

Chromodomain (CD)

Pre/post-SET

SET domain

Supplementary Figure 12: Sequence Features of Suv39h1. (**a**) Sequence alignment of the Suv39h1 N-terminus from indicated species reveals similarity with the DNA-binding helix of Gal4 (gray box). Cyan arrows denote Arg24 and Lys27, the putative chromatin binding residues of Suv39h1. The structure of the Gal4 zinc-finger bound to DNA is shown on the right (pdb code: 1D66) with the DNA binding residues highlighted. (**b**) Human Suv39h1 and its Yeast homolog Clr4 have different N-termini. The sequence alignment is annotated with domains for Suv39h1, and residues mutated in this study are highlighted with red arrows.

Supplementary Figure 13

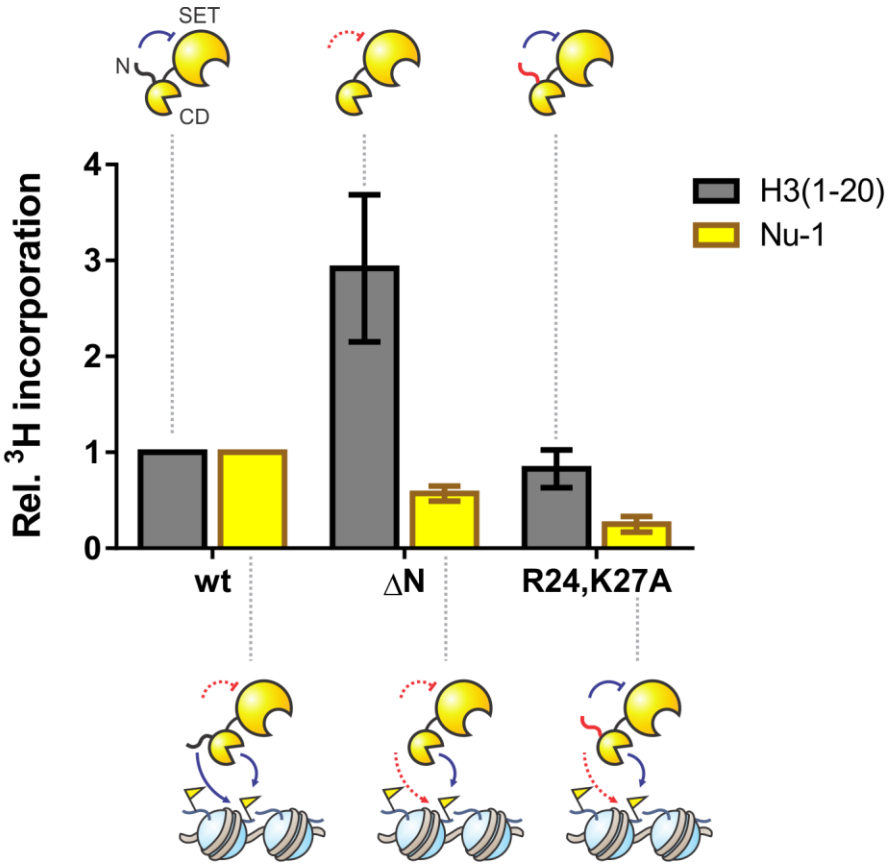

Supplementary Figure 13: Model for auto-inhibition by the N-terminus of Suv39h1. In the cartoon models, blue lines illustrate active feedback mechanisms, while red dashed lines represent masked pathways (due to mutation or previous activation steps). Note that the data in this figure are compiled from **Figures 2c** and **4c**.

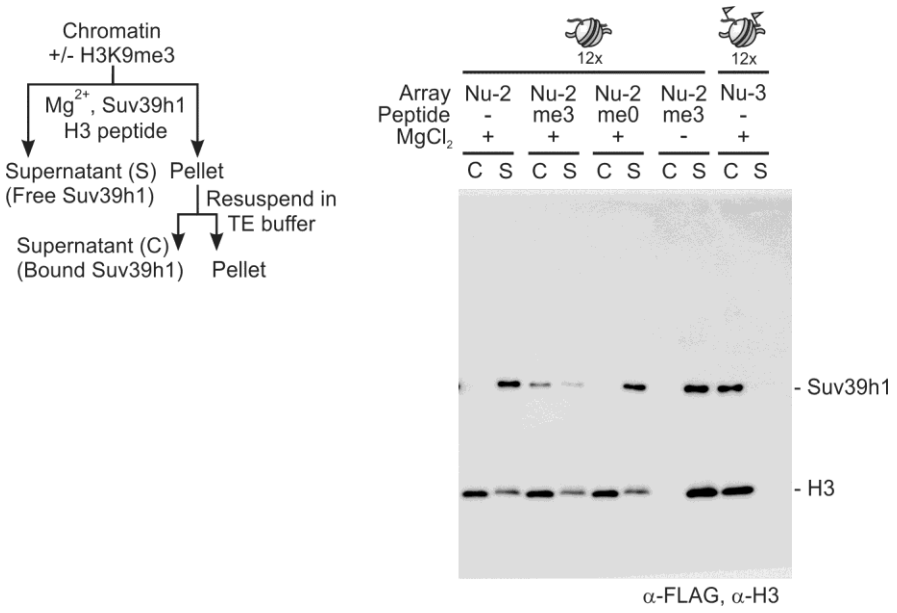

Supplementary Figure 14: The H3K9me3 mark promotes chromatin binding in *cis* and in *trans* (Extended version of Fig 3c). Western blot of a binding assay of wild-type Suv39h1 with array **Nu-2** or **Nu-3**. Where appropriate, H3 peptides are added at a concentration of 0.2 µM. A control reaction in the absence of $MgCl_2$ is included (lanes 7 and 8). A schematic workflow is indicated on the left.